

# The Multiscale Top-Hat Tensor Enables Specific Enhancement of Curvilinear Structures in 2D and 3D Images

Shuaa S. Alharbi<sup>a,b</sup>, Çiğdem Sazak<sup>a</sup>, Carl J. Nelson<sup>c</sup>, Haifa F. Alhasson<sup>a,b</sup>, Boguslaw Obara<sup>a,\*</sup>

<sup>a</sup>*Department of Computer Science, Durham University, UK*

<sup>b</sup>*Computer College, Qassim University, Qassim, KSA*

<sup>c</sup>*School of Physics and Astronomy, Glasgow University, UK*

---

## Abstract

Quantification and modelling of curvilinear structures in 2D and 3D images is a common challenge in a wide range of biomedical applications. Image enhancement is a crucial pre-processing step for curvilinear structure quantification. Many of the existing state-of-the-art enhancement approaches still suffer from contrast variations and noise. In this paper, we propose to address such problems via the use of a multiscale image processing approach, called Multiscale Top-Hat Tensor (MTHT). MTHT produces a better quality enhancement of curvilinear structures in low contrast and noisy images compared with other approaches in a range of 2D and 3D biomedical images. The proposed approach combines multiscale morphological filtering with a local tensor representation of curvilinear structure. The MTHT approach is validated on 2D and 3D synthetic and real images, and is also compared to the state-of-the-art curvilinear structure enhancement approaches. The obtained results demonstrate that the proposed approach provides high-quality curvilinear structure enhancement, allowing high accuracy segmentation and quantification in a wide range of 2D and 3D image datasets.

*Keywords:* Curvilinear Structures; Image Enhancement; Mathematical Morphology; Top-Hat; Tensor Representation; Vesselness; Neuriteness.

---

## 1. Introduction

The enhancement and detection of curvilinear structures are important and essential tasks in biomedical image processing. There is a wide range of curvilinear structure in biomedical imaging data, such as blood vessels, neurons, leaf veins, and fungal networks. Curvilinear structure enhancement is an important step, especially where the subjective quality of images of curvilinear structures is necessary for human interpretation.

A wide range of curvilinear structure enhancement approaches have used mathematical morphology operations to enhance curvilinear structures in 2D and 3D images. The top-hat transform [1] is a popular approach, which extracts bright features from a dark background that match the shape and orientation of a specified structuring element [2]. This approach has been used to extract curvilinear structures in retinal [3] and fingerprint [4] images. A local tensor representation [5] of an image measures how image structures change across dominant directions, and the eigenvalues and eigenvectors of the tensor can provide information that can be used to enhance, extract and analyse curvilinear structures. In this paper, we proposed a

new method, called Multiscale Top-Hat Tensor (MTHT), which combine these two approaches by representing curvilinear structures filtered by morphological operations in a local tensor representation of the image. In this method, We apply a multiscale top-hat with a line structuring element at different scales and orientations. Then, we produce a stack of top-hat images and combine them into a local tensor, find the eigenvalues to calculate vesselness and neuriteness to enhance the curvilinear structure in the biomedical images. This approach works with 2D and 3D images. Compared with other existing approaches, the gathered results prove that our proposed approach achieves high-quality curvilinear structure enhancement in the synthetic examples and in a wide range of real 2D and 3D biomedical image types. Further, images enhanced by MTHT show better curvilinear structure segmentation, as demonstrated by higher specificity and accuracy of the segmentation result when compared to existing enhancement approaches.

## 2. Related Work

### 2.1. Multiscale Process of Curvilinear Structures

The use of an image at a suitable scale usually avoids pre-processing stages with a high computational cost. It is also possible to deal explicitly with the scale parameter,

---

\*Corresponding author: Tel.: +44 (0) 191 33 42431;

Email address: boguslaw.obara@durham.ac.uk  
(Boguslaw Obara )

thus allowing the extraction of the significant image structures that become explicit at each level. In particular, an inherent property of the real world image, in this paper (curvilinear structure), is that they only exist as meaningful entities over certain ranges of scale. In particular, the curvilinear structures can appear at different scales and directions in real word images. This required a multiscale process to extract theses structures either by altering the image size, e.g. in a Gaussian pyramid [6] or by altering the filter size to enhance the different thickness of the vessel [7, 8].

Many curvilinear structure enhancement approaches for 2D and 3D images for a wide range of applications have been proposed in the literature to date. In this section, we list a small selection of the most relevant approaches divided into several subclasses according to the underlying concepts:

## 2.2. Hessian Matrix-based Approaches

A Hessian matrix-based image representation is constructed using responses of an image convolution with a set of matching filters, defined by second-order derivatives of the Gaussian at multiple scales [7, 9]. This concept is used to enhance and detect curve / tubular, sheet-like, and blob-like structures in the 2D and 3D images by exploring the relationships between eigenvectors and eigenvalues of the Hessian matrix. The three most common measurements proposed to date are: vesselness, neuriteness, and regularised volume ratio.

### 2.2.1. Vesselness

The vesselness measure [7] is calculated by computing the ratio of the eigenvalues of the Hessian matrix. The vesselness reaches its maximum when the scale and orientation of the filter matches the size and orientation of the local curvilinear structure. However, vesselness fails at junctions of curvilinear structures / networks due to the low filters responses.

### 2.2.2. Neuriteness

On the other hand, the neuriteness measure [9] is based on a slightly modified Hessian matrix by adding a new tuning parameter. Neuriteness, in the same way as vesselness, fails at junctions of curvilinear structures / networks due to the low filters responses.

### 2.2.3. Volume Ratio-based Approach

Hessian-based approaches rely on the eigenvalues and this leads to several problems: (1) eigenvalues are non-uniform throughout an elongated or rounded structure that has uniform intensity; (2) eigenvalues vary with image intensity; and (3) enhancement is not uniform across scales. A recent volume ratio-based approach [10] aims to solve such problems by computing the ratio of Hessian eigenvalues to handle the low magnitudes of eigenvalues and uniform responses across different structures. This

approach intends to intimate vascular elongated structures in 2D and 3D angiography images. However, it has drawbacks; despite enhancing the curvilinear structures, it also enhances the noise.

## 2.3. Mathematical Morphology-based Approaches

Morphological operations probe an image with a structuring element placed at all possible locations in the image and match it with the corresponding neighbourhood of pixels. This structuring element applied to an input image uses a set of operators (intersection, union, inclusion, complement). Morphological operations are easy to implement and are suitable for many shape-oriented problems. A great number of approaches have been proposed to enhance and detect the curvilinear structures based on different mathematical morphological transforms such as [11, 2, 12, 13, 14].

### 2.3.1. Top-Hat Transform

The top-hat transform has been widely used to enhance and detect curvilinear structures in retinal [2] and aerial [15] images. Zana and Klein [2] enhance the curvilinear structures using the top-hat transform with line structuring elements at different directions and with a fixed scale. Then, they computed the sum of the top-hat along each direction, followed by a curvature measure that is calculated using a Laplacian of Gaussian. Thus, any small bright noise will be reduced and the contrast of curvilinear structures will be improved.

### 2.3.2. Path Operators Transform

A mathematical morphology-based path opening and closing operation to detect the curvilinear structures in retinal images was introduced by [12]. Recently, a new path operator called Ranking the Orientation Responses of Path Operators (RORPO) has been proposed to distinguish curvilinear objects from blob-like and planar structures in images [13, 14]. The main disadvantage of the RORPO approach is its high computation cost when applied to large volume image datasets. Furthermore, this approach required an isotropic image resolution.

## 2.4. Phase Congruency Tensor-based Approaches

Phase congruency (PC) was first introduced in [16] and later combined with a local tensor to enhance curvilinear structures in 2D [17] and 3D [18] images. The majority of Hessian-based approaches rely on image intensity, which leads to poor enhancement or suppression of finer and lower intensity vessels, where Phase Congruency Tensor-based approaches are image contrast-independent. Moreover, the local tensor has a better representation of directions and the main advantage of using the local tensor is its ability to detect structures oriented in any direction. However, a major drawback of the PC-based concept is the complexity of its parameter space.

### 2.5. Histogram-based Approaches

Histogram-based approaches are the most popular technique for improving image contrast. Contrast Limited Adaptive Histogram Equalisation (CLAHE) [19] is a widely used pre-processing stage in order to improve the local details of an image. A major drawback of this method is its sensitivity to noise. An improvement proposed by [20] employs the anisotropic diffusion filter to reduce the noise and smooth the image, especially near the boundary.

### 2.6. Multiscale Line Detector-based Approaches

Nguyen et al. [21] proposed a multiscale curvilinear structure algorithm for vessel extraction from retinal images based on the line detectors with different length. The proposed method provides a robust way of enhancement and then detection of the retinal vessels that are close to each other and with the presence of vessel central reflex (a light band along the centre of a vessel). In [22], to improve the curvilinear structure detection, an approach based on banks of filters defined by lines with variable lengths. All filter responses are weighted and then combined. Another approach proposed by [23] combined K-mean clustering with a multiscale line detection. The proposed method produces good results in both healthy and unhealthy retina images in terms of accuracy. Most recently, to detect the small vessel-like structures, [24] applied a line detector with different sizes and orientations. In addition, they proposed a weighted linear combination of individual line detector responses followed by a hysteresis threshold in order to obtain a connected vessel tree.

### 2.7. Kernel-based Approaches

Gaussian kernel-based concepts are widely used in image processing for image blurring [25], edge detection [26], contrast improvement [27, 28] and image denoising [29]. Since the calculation of the Gaussian kernel is fast, especially in multidimensional applications, its use for curvilinear structures enhancement and extraction is very common [30, 31]. Perona [26] introduced a Gaussian steerable kernel-based approach that detects the edge with a great spatial and angular accuracy. Shui et al. [27] proposed a noise-robust anisotropic Gaussian kernel-based approach which achieves a good edge detection performance especially in the noisy images. Such an approach allows for robust curvilinear structures enhancement at the junction. Xiao et al. [32] proposed a new Bi-Gaussian kernel-based method exploiting the use of kernels at different scales. Furthermore, [33] proposed a hand-crafted feature scale and curvature invariant ridge detector (SCIRD) defined by a bank of second-order directional derivatives of Gaussians kernel.

### 2.8. Wavelet Transform-based Approaches

The wavelet transform has been widely used for curvilinear structure enhancement in biomedical images. In [34],

the authors propose a new approach to enhance the curvilinear structures in fingerprint images by involving the second derivative of a Gaussian filter with a directional wavelet transform. Another approach combines the Discrete Wavelet Transform and morphological filter (opening and closing) to enhance curvilinear structures in MRI images [35]. In addition, two different wavelets in parallel were applied in [36] to achieve an enhanced high-resolution image. In [37], the authors proposed an approach exploring the isotropic undecimated wavelet transform. However, similar to Hessian-based approaches, wavelet transform-based approaches fail to enhance low-intensity and fine curvilinear structures.

### 2.9. Learning-based Approaches

Recently, a wide range of machine learning-based methods [38, 39, 40] were proposed to deal with the curvilinear structure enhancement and detection complexity in images. [38, 39] employed a trainable filter to enhance the blood vessel in retinal images. Unlike the majority of unsupervised filtering-based techniques, [38] replace the linear implementation of the predefined kernels with a non-linear filter called Bar-Combination of Shifted Filter Responses (B-COSFIRE). The B-COSFIRE is a trainable filter designed to detect curvilinear structures by combining the responses of Gabor filter. Where, [39] applied a stack of B-COSFIRE filters. Another approach, proposed by [40], combined three different well-known curvilinear structure enhancement filters using unsupervised fuzzy c-means clustering and median ranking methods. The machine learning especially the deep learning is more suitable to deal with the scene complexity problem in natural images. It is much faster at inference, but it is also much more expensive in terms of data collection. Particularly, it is prohibitively expensive to collect thousands of training examples and ground truth images (especially for 3D images). Besides, deep learning models have millions of parameters and require a different set of libraries and skills. It is a heavy duty tool requiring a deep learning software environment.

## 3. Method

In this section, we introduce the proposed approach that consolidates the advantages of mathematical morphology and local tensor representation to enhance curvilinear structures in 2D/3D images. Before explaining the proposed approach in detail, it is useful to provide some more background of the concepts that are applied in this paper.

### 3.1. Background

#### 3.1.1. Mathematical Morphology and the Top-Hat Transform

Mathematical morphology operations are a set of non-linear filtering methods, and almost all of them formed

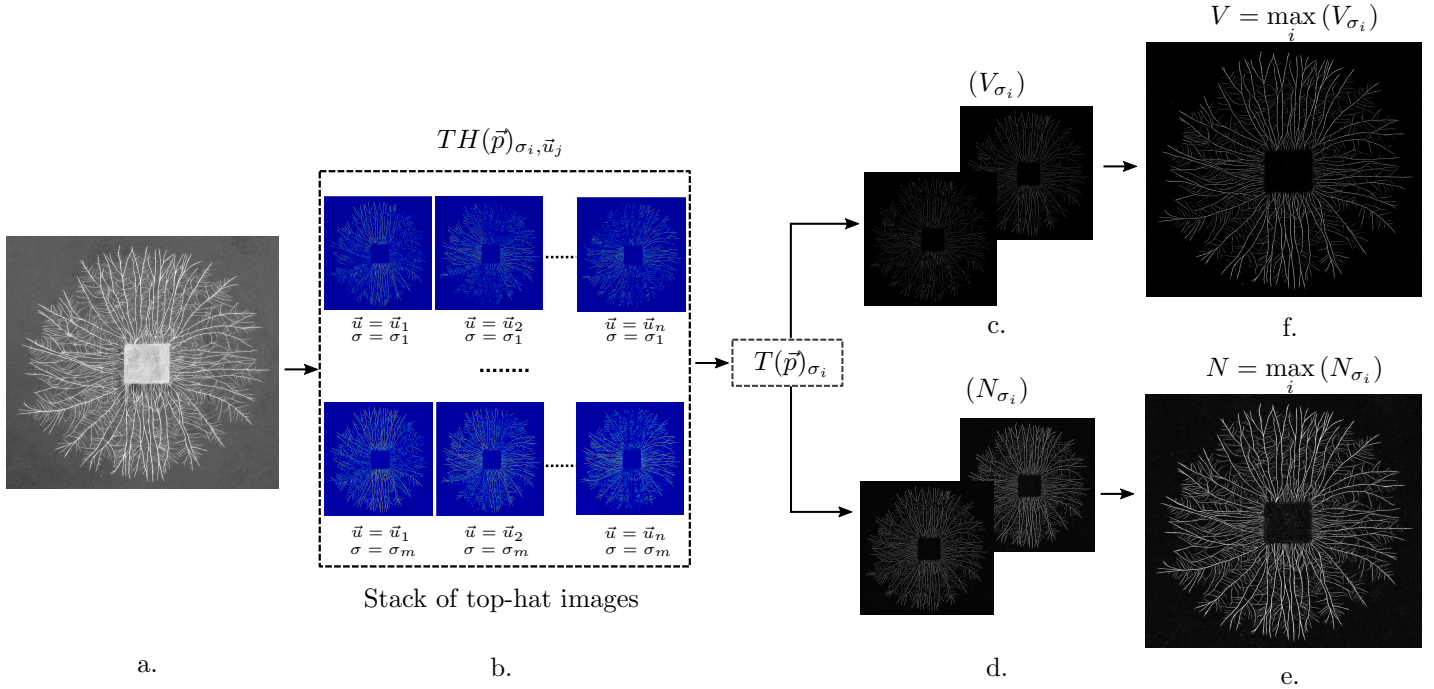


Figure 1: Workflow of the proposed approach: (a) Original image show the fungal network with a resolution of  $1494 \times 1620$  pixels [41]. (b) Stack of the top-hat images  $TH(\vec{p})_{\sigma_i, \vec{u}_j}$  produced using line structuring elements in different scale  $\sigma_i$  and orientations  $\vec{u}_j$ . (c-d) Vesselness and Neuriteness measurements at each scale  $\sigma_i$ . (e) MTHHT Vesselness, and (f) MTHHT Neuriteness.

through a combination of two basic operators: dilation and erosion.

If  $I(\vec{p})$  is a grey-scale image and  $B(\vec{p})$  is structuring element where  $\vec{p}$  denotes the pixel position  $[x, y]^T$  in the 2D images and  $[x, y, z]^T$  in the 3D images. Dilation, ( $\oplus$ ) can be defined as the maximum of the points in a weighted neighbourhood determined by the structuring element, and mathematically:

$$(I \oplus B)(\vec{p}) = \sup_{\mathbf{x} \in E} [I(\mathbf{x}) + B(\vec{p} - \mathbf{x})], \quad (1)$$

where ‘sup’ is the supremum and  $\mathbf{x} \in E$  denotes all points in Euclidean space within the image. Likewise, we mathematically represent erosion ( $\ominus$ ), as the minimum of the points in the neighbourhood determined by the structuring element:

$$(I \ominus B)(\vec{p}) = \inf_{\mathbf{x} \in E} [I(\mathbf{x}) + B(\vec{p} - \mathbf{x})], \quad (2)$$

where ‘inf’ is the infimum. The behaviour of dilation is expanding bright areas and reducing dark areas, while erosion is expanding dark regions reducing bright areas [1]. From these two operators we can define two further commonly used morphological filters:

$$\text{opening : } (I \circ B)(\vec{p}) = ((I \ominus B) \oplus B)(\vec{p}), \quad (3)$$

$$\text{closing : } (I \bullet B)(\vec{p}) = ((I \oplus B) \ominus B)(\vec{p}). \quad (4)$$

where an opening ( $\circ$ ) will preserve dark features and patterns, suppressing bright features, and a closing ( $\bullet$ ) will preserve bright features whilst suppressing dark patterns.

By comparing the original image and the result of opening or closing, two region extraction operations, which are called top-hat (TH) and bottom-hat (BH) transform, and defined as follows;

$$TH = I(\vec{p}) - (I \circ B)(\vec{p}), \quad (5)$$

$$BT = (I \bullet B)(\vec{p}) - I(\vec{p}). \quad (6)$$

The TH is usually used to extract bright structures, while BT is used to extract dark structures.

### 3.1.2. Vesselness and Neuriteness Measurements

**2D Vesselness:** One of the most popular Hessian-based approaches that used the eigenvalues of the Hessian to compute the likeliness of an image region to contain vessels or other image ridges [7]. It is computed based on the ratio of eigenvalues of the Hessian matrix as follows:

$$V_{\sigma} = \begin{cases} 0, & \lambda_2 > 0 \\ \exp\left(-\frac{R_{\beta}^2}{2\beta^2}\right) \left(1 - \exp\left(-\frac{S^2}{2c^2}\right)\right), & \text{otherwise} \end{cases} \quad (7)$$

where:

$$R_{\beta} = \lambda_1 / \lambda_2, \quad S = \sqrt{\lambda_1^2 + \lambda_2^2}.$$

The  $\lambda_1, \lambda_2$  are eigenvalues of the Hessian matrix, and  $\lambda_1 \geq \lambda_2$ . Where  $\beta$  and  $c$  are positive real user-defined parameters. If the magnitude of both eigenvalues is small, i.e. the local image structure is likely to be part of the background, then the vesselness measure will be small. If

one eigenvalue is small and the other large then the local structure is likely to be curvilinear and the vesselness measure is large. In case both of the eigenvalues magnitudes are large, then the structure is likely to be a blob and the vesselness measure will again small.

**3D Vesselness:** A 3D vesselness measure [7] is extended on the basis of all eigenvalues of the 3D Hessian matrix. Then, the vesselness for the 3D images is computed as follows:

$$V_\sigma = \begin{cases} 0, & \lambda_2, \lambda_3 > 0 \\ \exp\left(-\frac{R_\beta^2}{2\beta^2}\right)\left(1 - \exp\left(-\frac{R_\alpha^2}{2\alpha^2}\right)\right)\left(1 - \exp\left(-\frac{S^2}{2c^2}\right)\right), & \text{otherwise} \end{cases} \quad (8)$$

and where;

$$S = \sqrt{\lambda_1^2 + \lambda_2^2 + \lambda_3^2}, \quad R_\beta = \lambda_1/\sqrt{\lambda_2\lambda_3}, \quad R_\alpha = \lambda_2/\lambda_3.$$

Similar to vesselness measure in 2D, the  $\alpha$ ,  $\beta$  and  $c$  are real-valued positive user-defined parameters.

**2D Neuriteness:** This method introduced by [9] and designed to enhance low contrast and highly inhomogeneous neurites in the biomedical images. They changed the Hessian matrix by including a tuning parameter, alpha and derive two tuned eigenvalues  $\lambda_1'$  and  $\lambda_2'$  as follows:

$$\begin{aligned} \lambda_1' &= \lambda_1 + \alpha\lambda_2, \\ \lambda_2' &= \lambda_2 + \alpha\lambda_1. \end{aligned} \quad (9)$$

Then, they consider the maximum and minimum eigenvalues across the whole image as describe below, and define a new neurite-enhancing metric  $N_\sigma$ .

$$\begin{aligned} \lambda_{max} &= \max(|\lambda_1'|, |\lambda_2'|), \\ \lambda_{min} &= \min(\lambda_{max}). \end{aligned} \quad (10)$$

The neuriteness measurement define as:

$$N_\sigma = \begin{cases} \frac{\lambda_{max}}{\lambda_{min}} & \text{if } \lambda_{max} < 0 \\ 0 & \text{if } \lambda_{max} \geq 0 \end{cases}, \quad (11)$$

where  $\lambda_i'$  are symbolised the normalized eigenvalues of modify Hessian matrix. The  $\lambda_{min}$  denotes the smallest eigenvalue while  $\lambda_{max}$  represents the largest one of eigenvalues. Additionally, line like structures which is dark ( $\lambda_{max} \geq 0$ ) are ignored by the detector.

**3D Neuriteness:** The neuriteness measurement for the 3D image [9] can define using a 3D modified Hessian matrix. Then, the 3D neuriteness measurement can define as:

$$N_\sigma = \begin{cases} \frac{\lambda_{max}}{\lambda_{min}} & \text{if } \lambda_{max} < 0 \\ 0 & \text{if } \lambda_{max} \geq 0 \end{cases}, \quad (12)$$

and where;

$$\begin{aligned} \lambda_1' &= \lambda_1 + \alpha\lambda_2 + \alpha\lambda_3, \\ \lambda_2' &= \lambda_2 + \alpha\lambda_1 + \alpha\lambda_3, \\ \lambda_3' &= \lambda_3 + \alpha\lambda_1 + \alpha\lambda_2, \\ \lambda_{max} &= \max(|\lambda_1'|, |\lambda_2'|, |\lambda_3'|), \\ \lambda_{min} &= \min(\lambda_{max}). \end{aligned}$$

### 3.2. Proposed Method Framework

Since curvilinear structures can appear at different scales and directions in images, a top-hat transform using multi-scale and multi-directional structuring elements should be applied to detect them.

The image is processed by using line structuring elements of different sizes (scale) and directions (orientations) and is then represented as a tensor, the MTHT, which intrinsically contains information on scale and orientation. Then, through the use of its eigenvalues and eigenvectors, vesselness and neuriteness are calculated to enhance curvilinear structures. The workflow of our pipeline is shown in Figure 1. The details of the proposed approach are given below.

#### 3.2.1. Multiscale Top-Hat Transform

For a given 2D (or 3D) greyscale image  $I(\vec{p})$ , where  $\vec{p}$  is the pixel position, i.e.  $\vec{p} = (x, y)$ , a stack of 2D (or 3D) line structuring elements,  $B_{\sigma_i, \vec{u}_j}$  is defined. Here  $\sigma_i$  is the line structuring element length at scale  $i < m$  different scales,  $\vec{u}_j$  is the orientation vector  $j$  where  $j \leq n$ . While the number of orientations could be increased/decreased based on the number of scales used, we found that using greater than  $n = 12$  orientations in 2D and 3D images produced little improvement in enhancement (see also [2]).

In 2D, the  $\vec{u}_j$  orientation of line structuring element is defined as follows:

$$\vec{u}_j = [\cos(\theta_j), \sin(\theta_j)]^T, \quad (13)$$

where  $\theta_j \in [0; 180)$ .

In 3D, as proposed in [42, 18], a point distribution on the sphere of unit radius is used to define the orientation  $\vec{u}_j$  of the 3D line structuring element as follows:

$$\vec{u}_j = [\sin(\theta_j)\cos(\phi_j), \sin(\theta_j)\sin(\phi_j), \cos(\theta_j)]^T, \quad (14)$$

where  $\theta_j \in [0; 180)$  and  $\phi_j \in [0; 360)$ .

Then, we produced a top-hat image using a line structuring element defined by scale  $\sigma_i$  and orientation  $\vec{u}_j$  as follows:

$$TH(\vec{p})_{\sigma_i, \vec{u}_j} = I(\vec{p}) - (I \circ B_{\sigma_i, \vec{u}_j})(\vec{p}). \quad (15)$$

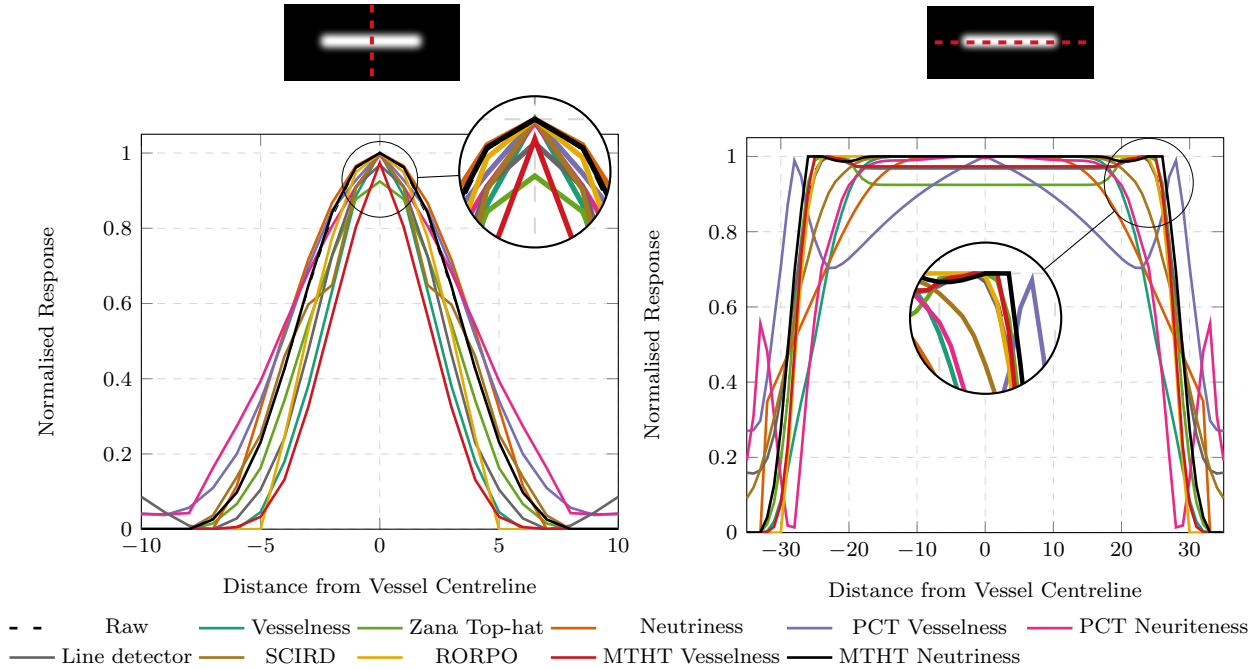


Figure 2: Cross-sectional profile of a 2D synthetic vessel image (black, dashed line), orthogonal profile in vessel-like structure enhanced by the proposed methods (black and red solid line) and by the state-of-the-art methods (see legend for colours). All images were normalised such that the brightest pixel in the whole image has a value of 1 and the darkest a value of 0.

### 3.2.2. Tensor Representation

In general, the tensor representation of an image can provide information about how much the image differs along and across the dominant orientations within a particular region [5].

In our case, the local tensor  $T(\vec{p})_{\sigma_i}$  representation of an image  $I(\vec{p})$  is generated by combining the bank of top-hat images from Equation 15 as follows:

$$T(\vec{p})_{\sigma_i} = \sum_{j=1}^n \|TH(\vec{p})_{\sigma_i, \vec{u}_j}\| (\vec{u}_j \vec{u}_j^T). \quad (16)$$

### 3.2.3. MTHT Vesselness

As described in Section 2, piecewise curvilinear segments can be detected by analysing the relations between eigenvalues and eigenvectors of the locally calculated Hessian [7]. In a similar way [17], the vesselness of the proposed approach is defined where the eigenvalues of the Hessian matrix are substituted with those of the MTHT. Finally, multiscale vesselness, for a given set of  $m$  scales can be calculated as follows:

$$V = \max_i (V_{\sigma_i}). \quad (17)$$

### 3.2.4. MTHT Neuritiness

When combining the neuritiness with our approach, it is necessary to modify the neuritiness measurement introduced by [9] for 2D and 3D images respectively. In [9], they normalised eigenvalues correspondingly to the smaller absolute eigenvalue which is a negative value. Whereas, in

our approach, we used a morphological line structuring element instead of the second order derivative of the Gaussian function used by [9], so the smaller absolute eigenvalue will be equal to 0. The modified neuritiness equation is:

$$N_{\sigma_i} = \begin{cases} \frac{\lambda}{\lambda_{max}} & \text{if } \lambda > 0 \\ 0 & \text{if } \lambda = 0 \end{cases}, \quad (18)$$

where  $\lambda$  is the larger in the magnitude of the two eigenvalues  $\lambda_1$  and  $\lambda_2$  for 2D images or the larger in the magnitude of the three eigenvalues  $\lambda_1$ ,  $\lambda_2$  and  $\lambda_3$  for 3D images.  $\lambda_{max}$  denotes the largest  $\lambda$  over all pixels in the image. Similar to vesselness, a multiscale neuritiness can be calculated as:

$$N = \max_i (N_{\sigma_i}). \quad (19)$$

### 3.3. Computational Cost

This method is a multiscale process which requires enhancing the curvilinear structures using different line lengths. Furthermore, the proposed method has been implemented and tested in Matlab which makes it slower than some of the comparator methods, (see Table 1 in the supplementary materials). However, a C++ implementation could improve the cost time and make the proposed method faster. In addition, parallel computing and dividing the enhancement process into discrete parts (i.e. based on scale), this can improve the computational cost of the proposed method.

## 4. Results

In this section, we present quantitative and qualitative validations for the proposed approach against both synthetic and real-world 2D and 3D imaging data. We then compare the results with state-of-the-art approaches. As a metric of performance, we have used the Receiver Operating Characteristic (ROC) curve [43] and the Area Under the Curve (AUC). We use these two analyses to compare the results of vessel enhancement methods to a known ground truth. A higher AUC value indicates a better enhancement of curvilinear structures, with a value of 1 indicating that the enhanced image is identical to the GT image. The results from each enhancement approach in all experiments implement in this paper are normalised. Thus the brightest pixel in the whole image has a value equal to 1 and the darkest value equivalent to 0.

### 4.1. Synthetic Validation

#### 4.1.1. Profile Analysis

In this section, we analyse the profile of the proposed method using a 2D synthetic image and compare the result with the state-of-the-art methods. In the cross-sectional profile in Figure 2, it is clearly shown that the proposed MTHT based vesselness (red solid line) and neuriteness (black solid line) succeed in enhancing the centre pixel (i.e. ridge) in the structure compared with morphological-base approaches such as Zana’s top-hat (light green solid line). The MTHT-neuriteness keep the width of the structure without changing in the curve thickness; whereas, other methods shrink (i.e. RORPO methods-yellow solid line) or expand the thickness of the curve (i.e. in phase congruency-based methods-purple and pink solid line). On the other hand, the proposed method in the orthogonal profile has a uniform response along the curve structure compared with the other methods.

#### 4.1.2. Response to Uneven Background Illumination

Figure 3 shows the outcome of the proposed methods and state-of-the-art methods to an uneven illumination background scenario in a synthetic 2D images. MTHT vesselness and neuriteness are able to maintain a bright central junction without background or border effects. We note that MTHT neuriteness does show some sensitivity to the background illumination and this should be considered when choosing an algorithm to use. In the real world application of vessel enhancement, this scenario is a quite common and important issue.

#### 4.1.3. Noise Sensitivity

In this experiment, we measure the robustness of the proposed method against 4 different types of noise using a created 2D synthetic curve image with known ground truth. We apply additive Gaussian, speckle, salt & pepper and multi-frequency (cloud) noise with different PSNR that produced using a genetic optimisation algorithm [44]. The

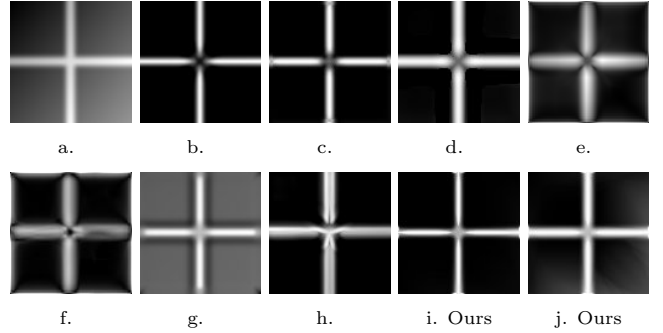


Figure 3: Comparison of the vessel enhancement methods’ abilities to deal with an uneven background illumination in a synthetic 2D image. (a) an input image, (b) vesselness, (c) Zana’s top-hat, (d) neuriteness, (e) PCT vesselness, (f) PCT neuriteness, (g) line detector, (h) SCIRD, (i) MTHT vesselness, and (j) MTHT neuriteness.

AUC is measured between each enhanced image from various methods and its ground truth and plot the results in Figure 6.

It is clear that the proposed method is sensitive to noise, this could be due to the sensitivity of the morphological operations to the different types of noise. On the other hand, unlike the kernel-based approach (i.e. SCIRD) which used a Gaussian smoothing function to reduce the noise, our method has not embedded with a noise elimination function to handle the noisy background. Further, combining the local tensor with the top-hat transform in the MTHT lead to slightly improve its result in terms of noise compared with Zana’s top-hat.

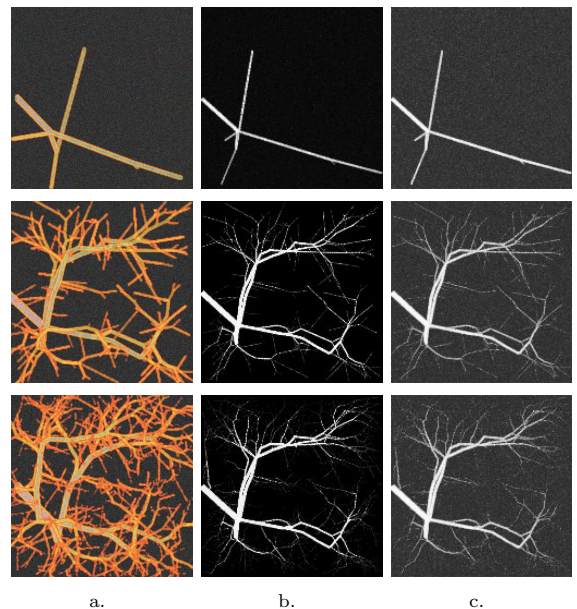


Figure 4: A selection of 3D synthetic vascular network images generated with the VasuSynth Software. Each image has a resolution of (167x167x167 voxels) and have different nodes to increase the complexity of structure. (a) Original images with different number of nodes (5, 200 and 1000) respectively. (b-c) are the enhance images from the proposed MTHT vesselness and MTHT neuriteness respectively.

Table 1: AUC values for the 9 vascular networks 3D images with increasing network’s complexity (see Figure 4) enhanced with the state-of-the-art approaches alongside the proposed MTHT vesselness and MTHT neuriteness.

Nodes	AUC						
	Vesselness [7]	Neuriteness [9]	PCT vesselness [18]	PCT neuritenss [18]	RORPO [14]	MTHT vesselness	MTHT neuriteness
5	0.999	0.923	0.840	0.897	0.999	<b>1.000</b>	0.992
10	0.996	0.883	0.820	0.873	0.997	<b>1.000</b>	0.998
50	0.976	0.830	0.794	0.851	0.965	<b>0.999</b>	0.982
100	0.951	0.778	0.778	0.827	0.930	<b>0.999</b>	0.988
200	0.930	0.755	0.770	0.799	0.900	<b>0.998</b>	0.981
400	0.910	0.746	0.749	0.788	0.879	<b>0.996</b>	0.975
600	0.902	0.743	0.742	0.777	0.869	<b>0.993</b>	0.970
800	0.885	0.719	0.724	0.756	0.855	<b>0.987</b>	0.959
1000	0.884	0.722	0.726	0.759	0.852	<b>0.983</b>	0.956
mean (StDev)	0.937 (0.045)	0.788 (0.073)	0.771 (0.040)	0.814 (0.050)	0.916 (0.058)	<b>0.995</b> (0.006)	0.978 (0.014)

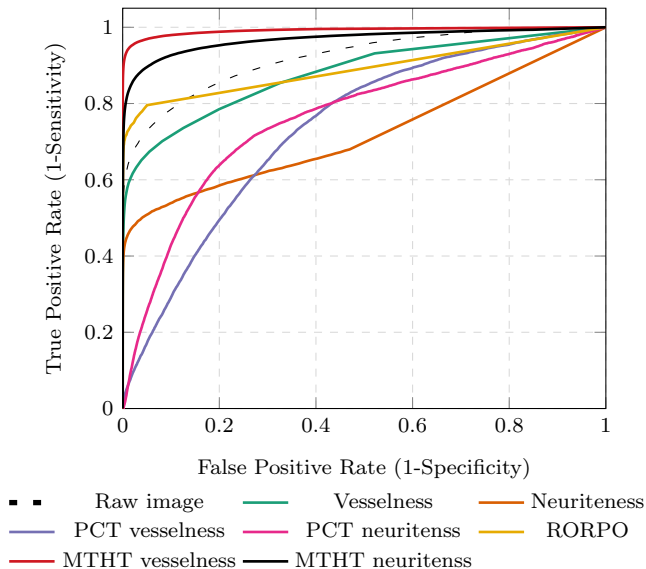


Figure 5: Mean ROC curve for all the 9 vascular networks 3D images enhanced using the state-of-the-art approaches alongside the proposed MTHT Vesselness and MTHT Neuriteness (see legend for colours). Correspondingly, the mean AUC values can be found in Table 1.

#### 4.1.4. 3D Vascular Network Complexity

In order to validate our approach in 3D, we used synthetic vascular networks produced by the free software package called VasuSynth [45]. The tree generation is performed by iteratively growing a vascular structure based on an oxygen demand map. Each generated image is associated with its ground truth. In this experiment, we generated 9 volumetric images with an increasing complexity and their corresponding ground truth. In addition, in order to make the image more realistic, we added a small amount of Gaussian noise of level  $\sigma^2 = 10$  and applied a Gaussian smoothing kernel with a standard deviation of 1. The results, in terms of AUC, are presented in Table 1 and a sample of the results are shown in Figure 4. We also demonstrate the mean ROC curve over

the 9 enhanced images, as shown in Figure 5. Our proposed approach is compared with vesselness [7], neuriteness [9], PCT (vesselness and neuriteness) [18] and with the latest 3D enhancement approach [14]. Our proposed approach clearly has the highest mean AUC value (0.995) with a standard deviation equal to (0.006) for the proposed MTHT-vesselness. On the other hand, we obtained an AUC value (0.978) with a standard deviation equal to (0.014) for the proposed MTHT-neuriteness compared to the state-of-art approaches.

## 4.2. Real-world Validation

### 4.2.1. Application to 2D Retinal Images

Although a visual inspection can provide some information regarding the effectiveness of the curvilinear structure enhancement approaches, a more rigorous form of quantitative validation is required. As in [10], we chose to use the Receiver Operating Characteristic (ROC) curve and the Area Under the Curve (AUC) metrics to compare the curvilinear structure enhancement approaches. We derive the ROC curve and then calculate the AUC value. Each enhanced image is segmented at different threshold levels and compared with the corresponding ground truth segmentation of curvilinear structures in the image. We measure the quality of the approach by using publicly available retinal image datasets: DRIVE [46], STARE [47] and HRF [48]. These datasets have been chosen because of their availability and their ground truth data. We have used these ground truth segmentations to quantitatively compare the proposed approach with the other curvilinear structure enhancement approaches.

In particular, we evaluate our approach, alongside the state-of-the-art methods, calculating the Receiver Operating Characteristic (ROC) curve and the mean of Area Under the Curve (AUC) between the enhanced images and the ground truth. The results are displayed accordingly in Figure 7 and Figure 8 and Table 2. An AUC with a value equal to 1 indicating that the enhanced image is identical to the ground truth image. Extra results from the DRIVE

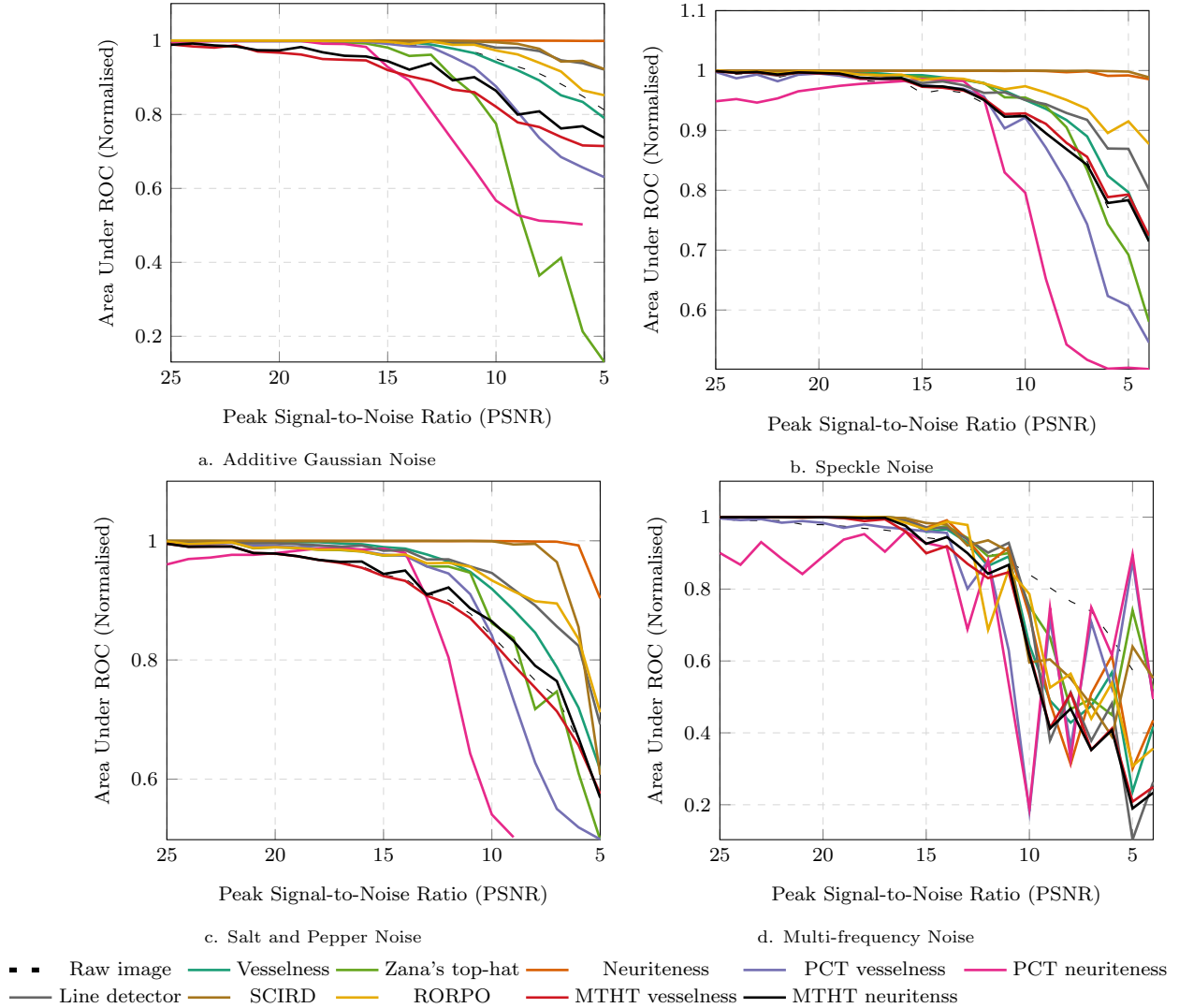


Figure 6: The mean AUC for the original 2D image (black, dashed line), the enhanced image under the proposed method (black and red, solid line) and the enhanced images under the comparator methods with different PSNRs for four different noise types: (a) additive Gaussian noise, (b) speckle noise, (c) salt and pepper noise, and (d) Multi-frequency Noise.

and STARE datasets can be found in the supplementary materials.

Our experimental results clearly show that our proposed approach works better than the state-of-the-art approaches for the STARE dataset. Furthermore, the proposed approach achieved a high score overall on the HRF healthy and unhealthy images, as illustrated in Table 2.

#### 4.2.2. Unhealthy Retina Image Difficulty

Due to the difficulties of some retinal 2D images in certain diseases such as diabetic retinopathy, we found it is useful to examine the MTHT methods behaviour in the unhealthy background subject. As shown in Figure 9, the proposed MTHT based neuriteness work better than MTHT-based vesselness in the unhealthy subject it still produces some noise in the background of the structure. In general, the proposed method outperformed other the-

state-of-the-art methods and achieved the highest overall score on the HRF unhealthy datasets as illustrated in Table 2.

#### 4.2.3. 2D and 3D Qualitative Validation

Additionally, as displayed in Figures 10 and 11, we have demonstrated the robustness of the proposed approach when applied to a wide range of 2D and 3D real-world images. Images showing dark objects on bright backgrounds are inverted before processing. It is clear that our approach has the best performance compared with the state-of-the-art approaches. In particular, our proposed approach can handle complex curvilinear networks as shown in Figure 11(1) and (2).

#### 4.2.4. Segmentation with Local Thresholding

As the enhancement phase is used mainly by various applications as a pre-processing step, we found it is use-

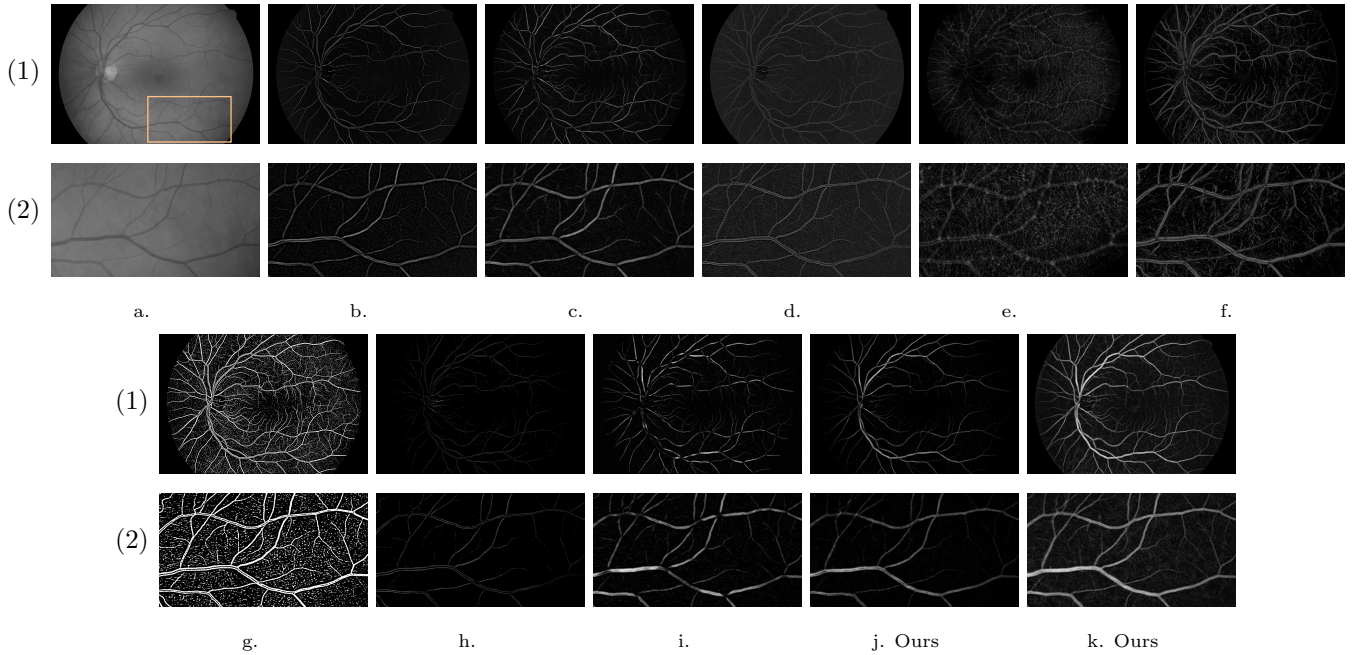


Figure 7: An example of a 2D retina image alongside the enhanced images from the state-of-the-art approaches. (a) Original grayscale images from the HRF retina dataset. The colour box indicates the region of interest (ROI). The zoomed region shows in row (2). (b) Vesselness [7], (c) Zana’s top-hat [2], (d) Neuriteness [9], (e) PCT vesselness [17], (f) PCT neuriteness [17], (g) line detector [21], (h) SCIRD [33], (i) RORPO [13], (j) MTHT vesselness, and (k) MTHT neuriteness.

Table 2: Mean AUC values for the state-of-the-art approaches and proposed MTHT vesselness and MTHT neuriteness across the DRIVE, STARE and HRF 2D retinal datasets. A section of results are shown in Figure 7 and the mean ROC curves can be seen in Figure 8.

Enhancement Approach	Year/Ref	AUC (StDev)			
		DRIVE	STARE	HRF (healthy)	HRF (unhealthy)
Raw image	-	0.416 (0.064)	0.490 (0.076)	0.530 (0.075)	0.541 (0.073)
Vesselness	1998 [7]	0.888 (0.243)	0.898 (0.215)	0.913 (0.020)	0.904 (0.020)
Zana’s top-hat	2001[2]	<b>0.933</b> (0.015)	0.956 (0.021)	0.943 (0.010)	0.910 (0.016)
Neuriteness	2004 [9]	0.909 (0.022)	0.927 (0.039)	0.896 (0.024)	0.879 (0.059)
PCT vesselness	2012 [17]	0.890 (0.037)	0.899 (0.056)	0.888 (0.011)	0.837 (0.030)
PCT neuriteness	2012 [17]	0.817 (0.121)	0.827 (0.165)	0.901 (0.029)	0.777 (0.022)
Line detector	2013 [21]	0.828 (0.024)	0.856 (0.042)	0.820 (0.022)	0.734 (0.026)
SCIRD	2015 [33]	0.925 (0.468)	0.946 (0.021)	0.956 (0.012)	0.692 (0.035)
RORPO	2017 [13]	0.867 (0.016)	0.902 (0.020)	0.869 (0.014)	0.854 (0.015)
MTHT vesselness	-	0.923 (0.017)	0.955 (0.024)	<b>0.959</b> (0.012)	0.934 (0.015)
MTHT neuriteness	-	0.931 (0.016)	<b>0.958</b> (0.019)	<b>0.959</b> (0.010)	<b>0.935</b> (0.018)

ful to examine the effectiveness of the MTHT methods for further image analysis (i.e. segmentation) using different 2D retinal datasets. In particular, a local thresholding approach [51] is applied to the enhanced images by the proposed method to obtain the segmented object. Then, we measure the performance quantitatively using three different evaluation matrices sensitivity (SE), specificity (SP)

and accuracy (ACC) [52, 53] given by:

$$SE = \frac{TP}{TP + FN}, \quad (20)$$

$$SP = \frac{TN}{TN + FP}, \quad (21)$$

$$ACC = \frac{TP + TN}{TP + TN + FP + FN}, \quad (22)$$

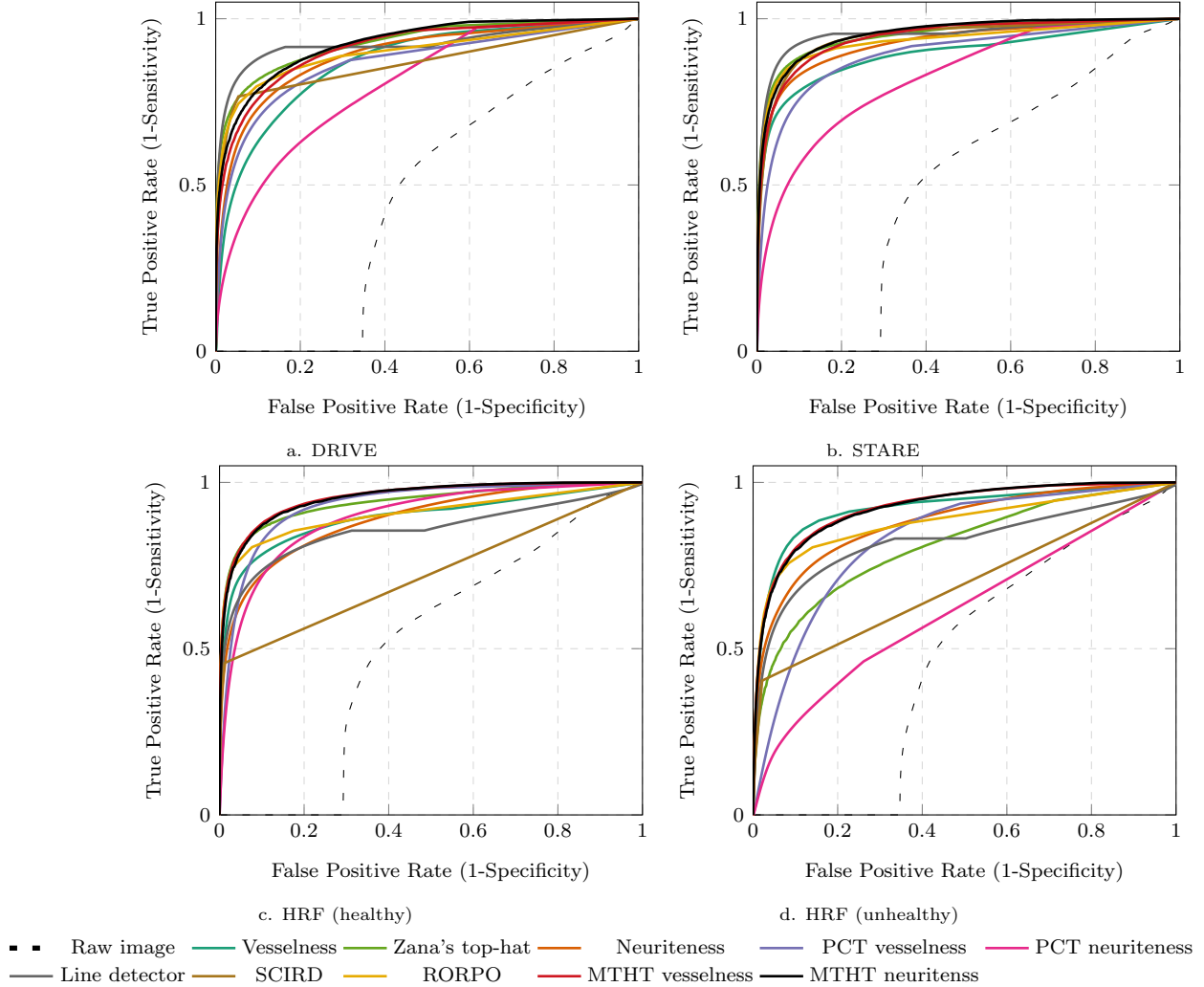


Figure 8: Mean ROC curves are calculated for all the 2D retinal images in: (a) DRIVE, (b) STARE, (c) HRF healthy, and (d) HRF unhealthy datasets enhanced using the state-of-the-art approaches alongside the proposed MTHT Vesselness and MTHT Neuriteness (see legend for colours). Correspondingly, the mean AUC values for all datasets can be found in Table 2.

where  $TP$  is the true positive count,  $FP$  the false positive count,  $TN$  the true negative and  $FN$  the false negative.

Table 3 illustrates published results of seventeen vessel segmentation methods and local segmentation after the proposed MTHT methods. The proposed MTHT methods provide more specific and more accurate segmentation results than other methods. It should be kept in mind that most of these methods have multiple stages, of which enhancement is just one of them, however, our methods can achieve such high-quality results with just an enhancement process. An example image from the HRF dataset segmentation results can be seen in Figure 12.

#### 4.2.5. Olfactory Projection Fibers 3D images

To demonstrate the stability of the proposed methods against noise in the 3D images, we apply our approach to Olfactory Projection Fibers image from DIADEM Challenge datasets [67]. We choose a sample image and add different levels of the Gaussian noise to it, (the noise levels

ranging  $\sigma = 10$  to  $\sigma = 60$ ). Then, we applied the proposed MTHT methods to this sample image and calculate the AUC values. Notice that, proposed methods have high AUC values against this type of the noise and display the results in Figure 13.

## 5. Implementation

The software was implemented and written in MATLAB 2017a on Windows 8.1 pro 64-bit PC running an Intel Core i7-4790 CPU (3.60 GHz) with 16GB RAM. The software is made available at: <https://github.com/ShuaaAlharbi/MTHT>.

## 6. Conclusion

The proposed MTHT approach is evaluated qualitatively and quantitatively using different 2D and 3D images.

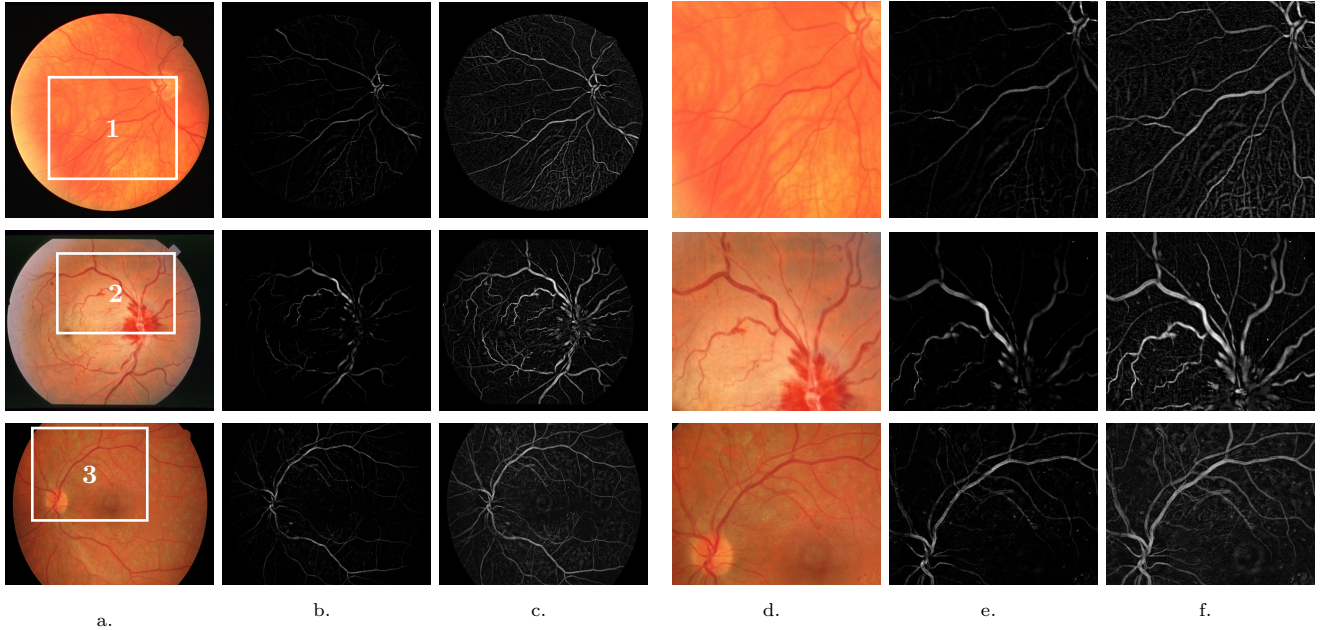


Figure 9: An illustration of the proposed method applying to unhealthy subjects of different retina 2D images. (a) Original image from DRIVE, STARE and HRF (Unhealthy) dataset respectively. The white box indicates the ROI. Results from the proposed method: (b) MHTH vesselness, and MHTH neuriteness (c). (d-f) Zoomed in the regions in 1, 2 and 3 in (a) alongside their results from proposed MHTH vesselness (e), and MHTH neuriteness (f).

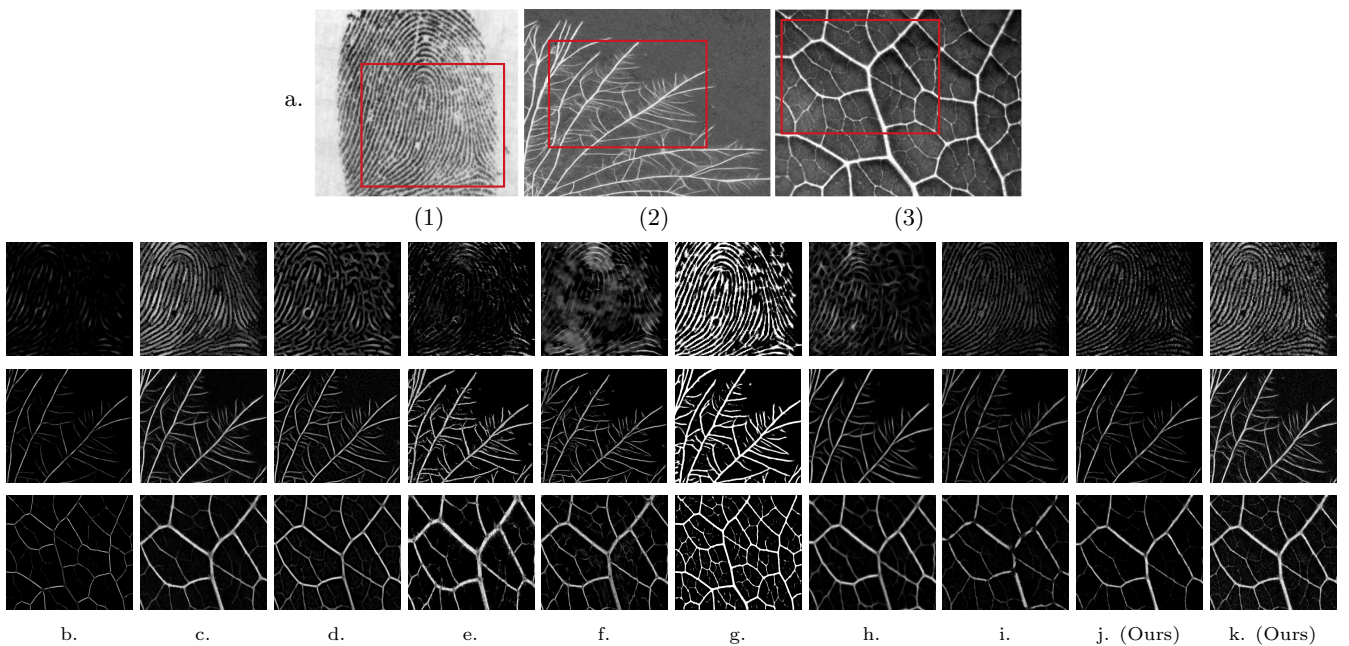


Figure 10: Comparison of the curvilinear structure enhancement approaches using 2D real images. (a) Original images: (1) finger print [49], (2) macro-scale networks (provided by Prof. M. Fricker, Oxford University, UK), and (3) leaf image [17]. The red box on the original image shows the ROI. (b) Vesselness [7], (c) Zana's top-hat [2], (d) Neuriteness [9], (e) PCT vesselness [17], (f) PCT neuriteness [17], (g) line detector [21], (h) SCIRD [33], (i) RORPO [13], (j) MHTH vesselness, and (k) MHTH neuriteness.

The experimental results show that the approach is comparable with the Hessian-based vesselness and neuriteness approaches, as well with the other state-of-art methods.

In general, the MHTH proposed approach showed better enhancement results compared with the state-of-art approaches especially in the challenging retinal datasets.

Furthermore, as shown in Table 3, the proposed MHTH method has compared with the segmentation methods and obtained better results in term of specificity (SP) and accuracy (ACC). Although the proposed approach achieves good enhancement results in all tested biomedical images, there is room for improvement. In particular, as shown

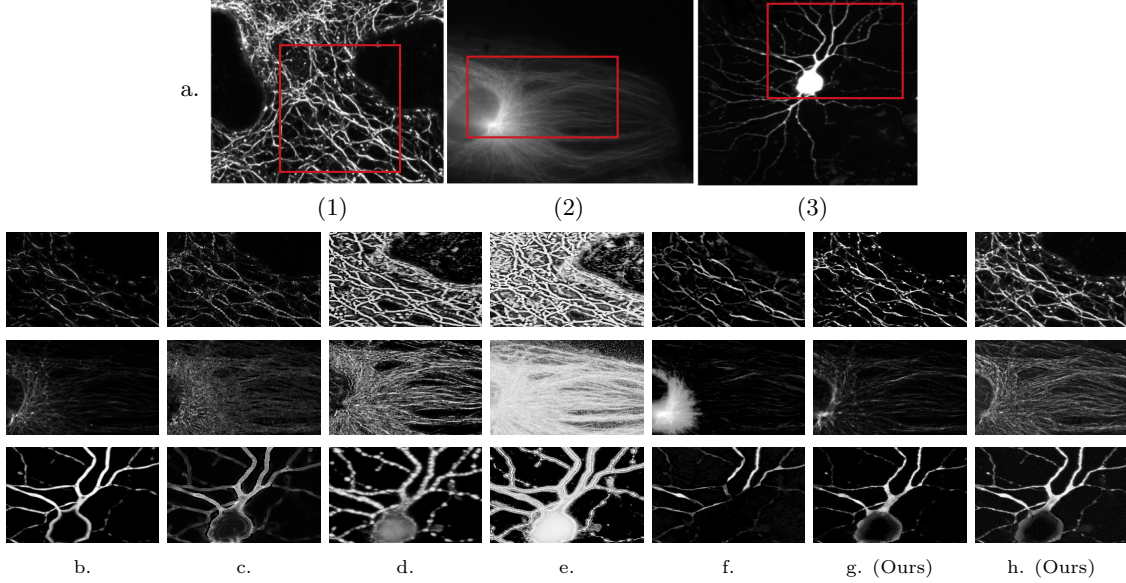


Figure 11: Comparison of the curvilinear structure enhancement approaches using 3D real images. (a) Original images: (1) keratin network in a skin cell (Dr Tim Hawkins, Durham University, UK), (2) microtubules [50], and (3) neuronal (provided by Dr Chris Banna, UC Santa Barbara, USA). The red box on the original image shows the ROI. (b) Vesselness [7], (c) Neuriteness [9], (d) PCT vesselness [18], (e) PCT neuriteness [18], (f) RORPO [14], (g) MTHT vesselness, and (h) MTHT neuriteness.

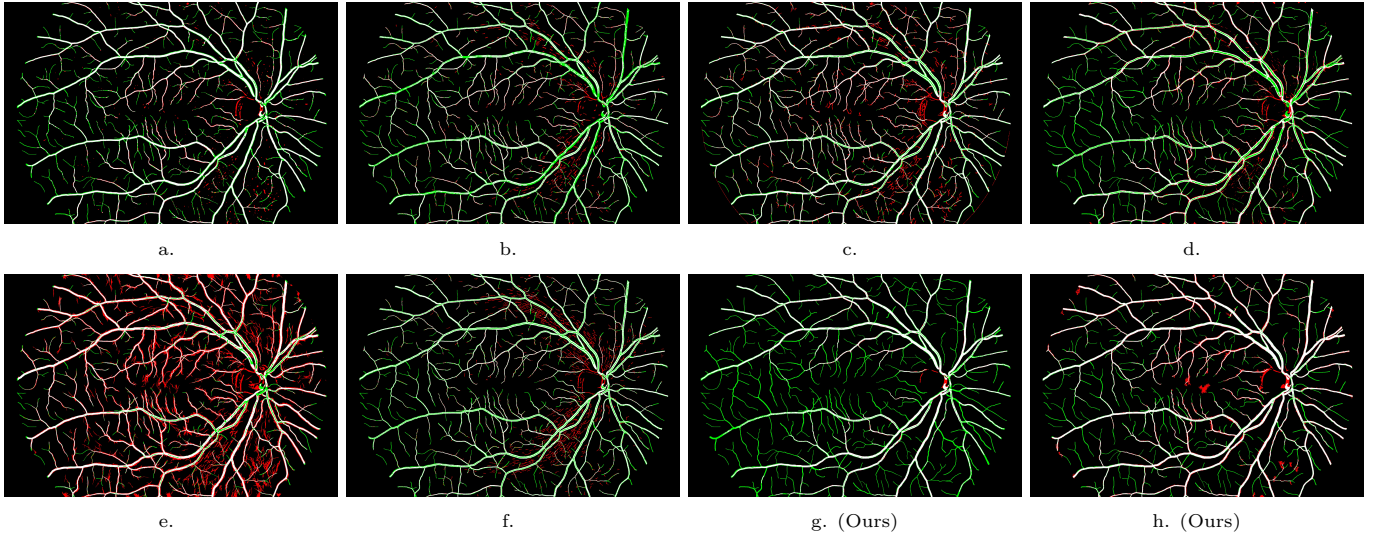


Figure 12: Vessel segmentation results obtained by the proposed and the state-of-the-art vessel-like structures enhancement methods followed by the same local thresholding approach proposed in [51] when applied to the HRF 2D retinal dataset images. (a) vesselness, (b) Zana's top-hat, (c) neuriteness, (d) PCT vesselness, (e) PCT neuriteness, (f) line detector, (g) MTHT vesselness, and (h) MTHT neuriteness. Colours indicate true positive (white), false positive (red) and false negative pixels (green).

in Figure 6, the MTHT method is sensitive to noise. The potential improvement involves using a noise suppression, (i.e. Gaussian kernel) which helps to reduce the noise in the image. On the other hand, using a combination of the structural elements in the implementation of the top-hat transform may improved enhancement of the image background, as well as better handling of junctions. These solutions should be explored further.

## Acknowledgement

Shuaa Alharbi and Haifa Alhasson are supported by the Saudi Arabian Ministry of Higher Education Doctoral Scholarship and Qassim University in Saudi Arabia. Çiğdem Sazak is funded by the Turkey Ministry of National Education. Carl J. Nelson is funded by EPSRC UK (EP/N509668/1).

Table 3: Performance of different vessel segmentation methods have been reported in the literature with the proposed method, regarding mean sensitivity (SE), specificity (SP), accuracy (ACC) on the all over the DRIVE, STARE and HRF 2D retinal datasets.

Method	DRIVE			STARE			HRF		
	SE (%)	SP (%)	ACC (%)	SE (%)	SP (%)	ACC (%)	SE (%)	SP (%)	ACC (%)
Staal et.al [54]	-	-	0.946	-	-	0.951	-	-	-
Soares et.al [55]	-	-	0.946	-	-	0.948	-	-	-
Lupascu et.al [56]	0.720	-	0.959	-	-	-	-	-	-
You et.al [57]	0.741	0.975	0.943	0.726	0.975	0.949	-	-	-
Marin et.al [58]	0.706	0.980	0.945	0.694	0.981	0.952	-	-	-
Wang et.al [59]	-	-	0.946	-	-	0.952	-	-	-
Mendonca et.al [60]	0.734	0.976	0.945	0.699	0.973	0.944	-	-	-
Palomera-Perez et.al [61]	0.660	0.961	0.922	0.779	0.940	0.924	-	-	-
Matinez-Perez et.al [62]	0.724	0.965	0.934	0.750	0.956	0.941	-	-	-
Al-Diri et.al [63]	0.728	0.955	-	0.752	0.968	-	-	-	-
Fraz et.al [64]	0.715	0.976	0.943	0.731	0.968	0.944	-	-	-
Nguyen et.al [21]	-	-	0.940	-	-	0.932	-	-	-
Bankhead et.al [37]	0.703	0.971	0.937	0.758	0.950	0.932	-	-	-
Orlando et.al [65]	0.785	0.967	-	-	-	-	-	-	-
Azzopardi et.al [38]	0.766	0.970	0.944	0.772	0.970	0.950	-	-	-
Odstrcilik et.al [48]	0.784	0.951	0.934	0.706	0.969	0.934	0.786	0.975	0.953
Zhang et.al [66]	0.774	0.972	0.947	0.779	0.975	0.955	0.797	0.971	0.955
MTHT Vesselness	0.619	0.989	<b>0.958</b>	0.638	0.987	<b>0.963</b>	0.819	0.971	<b>0.957</b>
MTHT Neuriteness	0.685	0.983	<b>0.957</b>	0.618	0.988	<b>0.962</b>	0.794	0.977	<b>0.960</b>

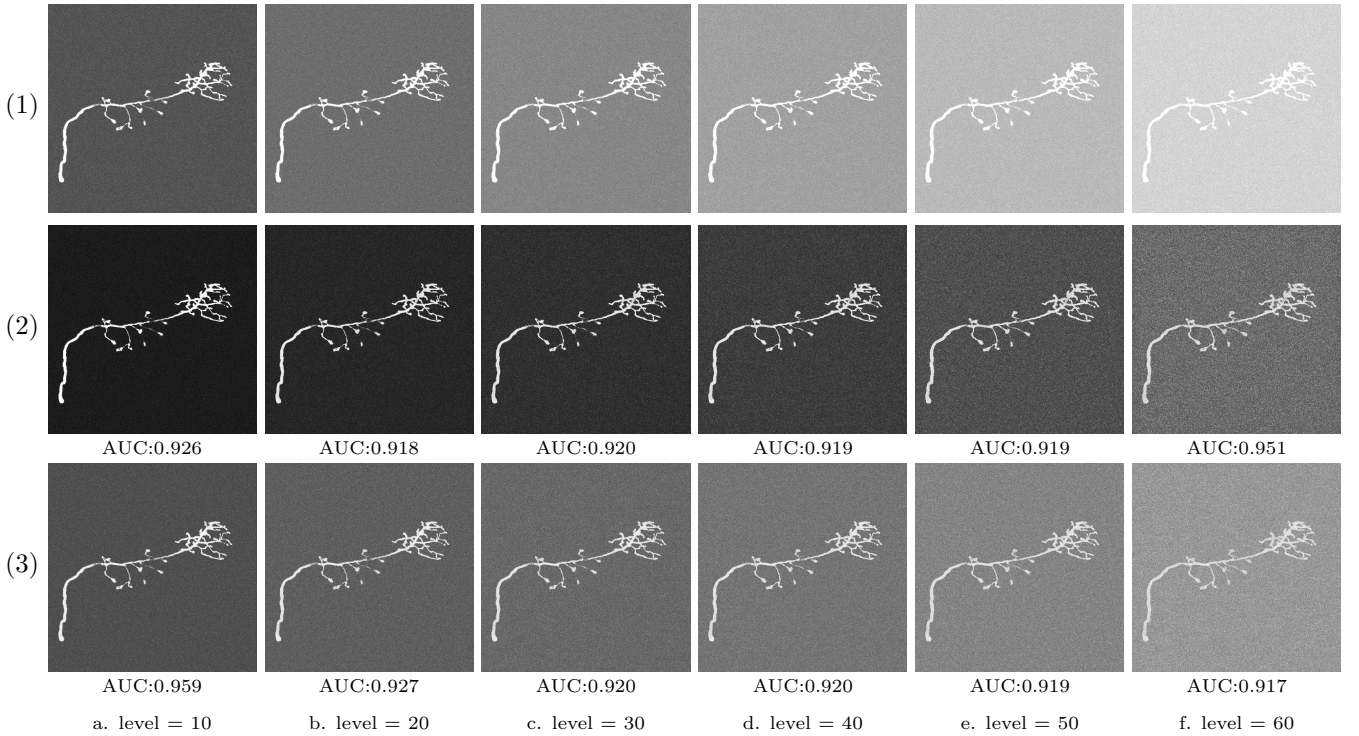


Figure 13: Application of the proposed method into the Olfactory Projection Neuron dataset from the DIADEM Challenge. All of the images are 2D maximum intensity projections. (1) Input images that have been contaminated by different levels (increasing left to right) of Gaussian additive noise. (2-3) The enhancement results from the proposed methods and corresponding AUC values of: (2) MTHT vesselness, and (3) the results from the MTHT neuriteness.

## References

- [1] R. M. Haralick, S. R. Sternberg, X. Zhuang, Image analysis using mathematical morphology, *IEEE Transactions on Pattern Analysis and Machine Intelligence* 1 (4) (1987) 532–550.
- [2] F. Zana, J.-C. Klein, Segmentation of vessel-like patterns using mathematical morphology and curvature evaluation, *IEEE Transactions on Image Processing* 10 (7) (2001) 1010–1019.
- [3] M. Liao, Y.-q. Zhao, X.-h. Wang, P.-s. Dai, Retinal vessel enhancement based on multi-scale top-hat transformation and histogram fitting stretching, *Optics and Laser Technology* 58 (2014) 56–62.
- [4] P. Bibiloni, M. González-Hidalgo, S. Massanet, General-purpose curvilinear object detection with fuzzy mathematical morphology, *Applied Soft Computing* 60 (2017) 655–669.
- [5] H. Knutsson, Representing local structure using tensors, in:

- Scandinavian Conference on Image Analysis, Oulu, Finland, 1989, pp. 244–251.
- [6] S. Paris, S. W. Hasinoff, J. Kautz, Local laplacian filters: Edge-aware image processing with a laplacian pyramid, *ACM Transactions on Graphics* 30 (4) (2011) 68–1.
  - [7] A. F. Frangi, W. J. Niessen, K. L. Vincken, M. A. Viergever, Multiscale vessel enhancement filtering, in: *International Conference on Medical Image Computing and Computer-Assisted Intervention*, Cambridge MA, USA, 1998, pp. 130–137.
  - [8] C. Lopez-Molina, G. V.-D. de Ulzurrun, J. Baetens, J. Van den Bulcke, B. De Baets, Unsupervised ridge detection using second order anisotropic gaussian kernels, *Signal Processing* 116 (2015) 55–67.
  - [9] E. Meijering, M. Jacob, J.-C. Sarría, P. Steiner, H. Hirling, M. Unser, Design and validation of a tool for neurite tracing and analysis in fluorescence microscopy images, *Cytometry* 58 (2) (2004) 167–176.
  - [10] T. Jerman, F. Pernuš, B. Likar, Ž. Špiclin, Enhancement of vascular structures in 3D and 2D angiographic images, *IEEE Transactions on Medical Imaging* 35 (9) (2016) 2107–2118.
  - [11] P. Soille, H. Talbot, Directional morphological filtering, *IEEE Transactions on Pattern Analysis and Machine Intelligence* 23 (11) (2001) 1313–1329.
  - [12] E. M. Sigursson, S. Valero, J. A. Benediktsson, J. Chanussot, H. Talbot, E. Stefánsson, Automatic retinal vessel extraction based on directional mathematical morphology and fuzzy classification, *Pattern Recognition Letters* 47 (2014) 164–171.
  - [13] O. Merveille, B. Naegel, H. Talbot, L. Najman, N. Passat, 2D filtering of curvilinear structures by ranking the orientation responses of path operators (RORPO), *Image Processing On Line* 7 (2017) 246–261.
  - [14] O. Merveille, H. Talbot, L. Najman, N. Passat, Curvilinear structure analysis by ranking the orientation responses of path operators, *IEEE Transactions on Pattern Analysis and Machine Intelligence* 40 (2) (2018) 304–317.
  - [15] J. C. M. Román, H. L. Ayala, J. L. V. Noguera, Top-hat transform for enhancement of aerial thermal images, in: *Brazilian Symposium on Computer Graphics and Image Processing*, Niterói, Brazil, 2017, pp. 277–284.
  - [16] P. Kovese, Phase congruency detects corners and edges, in: *The Australian Pattern Recognition Society Conference*, Brisbane, Australia, 2003, pp. 309–318.
  - [17] B. Obara, M. Fricker, D. Gavaghan, V. Grau, Contrast-independent curvilinear structure detection in biomedical images, *IEEE Transactions on Image Processing* 21 (5) (2012) 2572–2581.
  - [18] Ç. Sazak, B. Obara, Contrast-independent curvilinear structure enhancement in 3D biomedical images, in: *IEEE International Symposium on Biomedical Imaging*, Melbourne, Australia, 2017, pp. 1165–1168.
  - [19] E. D. Pisano, S. Zong, B. M. Hemminger, M. DeLuca, R. E. Johnston, K. Muller, M. P. Braeuning, S. M. Pizer, Contrast limited adaptive histogram equalization image processing to improve the detection of simulated spiculations in dense mammograms, *Journal of Digital Imaging* 11 (4) (1998) 193.
  - [20] Y. Q. Zhao, X. H. Wang, X. F. Wang, F. Y. Shih, Retinal vessels segmentation based on level set and region growing, *Pattern Recognition* 47 (7) (2014) 2437–2446.
  - [21] U. T. Nguyen, A. Bhuiyan, L. A. Park, K. Ramamohanarao, An effective retinal blood vessel segmentation method using multi-scale line detection, *Pattern Recognition* 46 (3).
  - [22] Y. Hou, Automatic segmentation of retinal blood vessels based on improved multiscale line detection, *Journal of Computing Science and Engineering* 8 (2) (2014) 119–128.
  - [23] V. M. Saffarzadeh, A. Osareh, B. Shadgar, Vessel segmentation in retinal images using multi-scale line operator and K-means clustering, *Journal of Medical Signals and Sensors* 4 (2) (2014) 122.
  - [24] M. A. Khan, T. M. Khan, D. Bailey, T. A. Soomro, A generalized multi-scale line-detection method to boost retinal vessel segmentation sensitivity, *Pattern Analysis and Applications* 1 (1) (2018) 1–20.
  - [25] M. S. Nixon, A. S. Aguado, *Feature extraction & image processing for computer vision*, Academic Press, 2012.
  - [26] P. Perona, Steerable-scalable kernels for edge detection and junction analysis, in: *European Conference on Computer Vision*, Santa Margherita Ligure, Italy, 1992, pp. 3–18.
  - [27] P.-L. Shui, W.-C. Zhang, Noise-robust edge detector combining isotropic and anisotropic Gaussian kernels, *Pattern Recognition* 45 (2) (2012) 806 – 820.
  - [28] M. Abdoli, H. Sarikhani, M. Ghanbari, P. Brault, Gaussian mixture model-based contrast enhancement, *IET Image Processing* 9 (7) (2015) 569–577.
  - [29] J. Portilla, V. Strela, M. J. Wainwright, E. P. Simoncelli, Image denoising using scale mixtures of Gaussians in the wavelet domain, *IEEE Transactions on Image Processing* 12 (11) (2003) 1338–1351.
  - [30] W. T. Freeman, E. H. Adelson, Steerable filters for early vision, image analysis, and wavelet decomposition, in: *IEEE International Conference on Computer Vision*, Osaka, Japan, 1990, pp. 406–415.
  - [31] W. T. Freeman, Steerable filters and local analysis of image structure, Tech. rep., DTIC Document (1992).
  - [32] C. Xiao, M. Staring, Y. Wang, D. P. Shamonin, B. C. Stoel, Multiscale bi-Gaussian filter for adjacent curvilinear structures detection with application to vasculature images, *IEEE Transactions on Image Processing* 22 (1) (2013) 174–188.
  - [33] R. Annunziata, A. Kheirkhah, P. Hamrah, E. Trucco, Scale and curvature invariant ridge detector for tortuous and fragmented structures, in: *International Conference on Medical Image Computing and Computer-Assisted Intervention*, Munich, Germany, 2015, pp. 588–595.
  - [34] K. Sihalath, S. Choomchuay, S. Wada, K. Hamamoto, Fingerprint image enhancement with second derivative Gaussian filter and directional wavelet transform, in: *International Conference on Computer Engineering and Applications*, Bali Island, Indonesia, 2010, pp. 112–116.
  - [35] A. Srivastava, A. Raj, V. Bhateja, et al., Combination of wavelet transform and morphological filtering for enhancement of magnetic resonance images, in: *Digital Information Processing and Communications*, Springer, 2011, pp. 460–474.
  - [36] H. Demirel, G. Anbarjafari, Image resolution enhancement by using discrete and stationary wavelet decomposition, *IEEE Transactions on Image Processing* 20 (5) (2011) 1458–1460.
  - [37] P. Bankhead, C. N. Scholfield, J. G. McGeown, T. M. Curtis, Fast retinal vessel detection and measurement using wavelets and edge location refinement, *PLoS One* 7 (3) (2012) e32435.
  - [38] G. Azzopardi, N. Strisciuglio, M. Vento, N. Petkov, Trainable COSFIRE filters for vessel delineation with application to retinal images, *Medical Image Analysis* 19 (1) (2015) 46–57.
  - [39] N. Strisciuglio, G. Azzopardi, M. Vento, N. Petkov, Supervised vessel delineation in retinal fundus images with the automatic selection of B-COSFIRE filters, *Machine Vision and Applications* 27 (8) (2016) 1137–1149.
  - [40] W. S. Oliveira, J. V. Teixeira, T. I. Ren, G. D. Cavalcanti, J. Sijbers, Unsupervised retinal vessel segmentation using combined filters, *PLoS one* 11 (2) (2016) e0149943.
  - [41] B. Obara, M. Fricker, V. Grau, A bioimage informatics approach to automatically extract complex fungal networks, *Bioinformatics* 28 (18) (2012) 2374–2381.
  - [42] I. Hacihaliloglu, R. Abugharbieh, A. J. Hodgson, R. N. Rohling, 2A-4 Enhancement of bone surface visualization from 3D ultrasound based on local phase information, in: *IEEE International Ultrasonics Symposium*, Vancouver, Canada, 2006, pp. 21–24.
  - [43] T. Fawcett, An introduction to ROC analysis, *Pattern Recognition Letters* 27 (8) (2006) 861–874.
  - [44] D. E. Goldberg, J. H. Holland, Genetic algorithms and machine learning, *Machine Learning* 3 (2) (1988) 95–99.
  - [45] G. Hamarneh, P. Jassi, Vascusynth: simulating vascular trees for generating volumetric image data with ground-truth segmentation and tree analysis, *Computerized Medical Imaging and Graphics* 34 (8) (2010) 605–616.

- [46] M. Niemeijer, J. Staal, B. van Ginneken, M. Loog, M. D. Abramoff, Comparative study of retinal vessel segmentation methods on a new publicly available database, in: *Image Processing in Medical Imaging*, San Diego, CA, 2004, pp. 648–657.
- [47] A. Hoover, V. Kouznetsova, M. Goldbaum, Locating blood vessels in retinal images by piecewise threshold probing of a matched filter response, *IEEE Transactions on Medical Imaging* 19 (3) (2000) 203–210.
- [48] J. Odstrcilik, R. Kolar, A. Budai, J. Hornegger, J. Jan, J. Gazarek, T. Kubena, P. Cernosek, O. Svoboda, E. Angelopoulou, Retinal vessel segmentation by improved matched filtering: evaluation on a new high-resolution fundus image database, *IET Image Processing* 7 (4) (2013) 373–383.
- [49] D. Maltoni, D. Maio, A. K. Jain, S. Prabhakar, *Handbook of Fingerprint Recognition*, Springer Science & Business Media, 2009.
- [50] E. D. Gelasca, J. Byun, B. Obara, B. Manjunath, Evaluation and benchmark for biological image segmentation, in: *IEEE International Conference on Image Processing*, San Diego, CA, 2008, pp. 1816–1819.
- [51] X. Jiang, D. Mojon, Adaptive local thresholding by verification-based multithreshold probing with application to vessel detection in retinal images, *IEEE Transactions on Pattern Analysis and Machine Intelligence* 25 (1) (2003) 131–137.
- [52] J. Yerushalmy, Statistical problems in assessing methods of medical diagnosis, with special reference to X-ray techniques, *Public Health Reports* 1 (1) (1947) 1432–1449.
- [53] D. M. Powers, Evaluation: From precision, recall and f-factor to ROC, informedness, markedness & correlation, *Journal of Machine Learning Technologies* 2 (1) (2011) 37–63.
- [54] J. Staal, M. Abramoff, M. Niemeijer, M. Viergever, B. van Ginneken, Ridge based vessel segmentation in color images of the retina, *IEEE Transactions on Medical Imaging* 23 (4) (2004) 501–509.
- [55] J. V. Soares, J. J. Leandro, R. M. Cesar, H. F. Jelinek, M. J. Cree, Retinal vessel segmentation using the 2-D Gabor wavelet and supervised classification, *IEEE Transactions on Medical Imaging* 25 (9) (2006) 1214–1222.
- [56] C. A. Lupascu, D. Tegolo, E. Trucco, Fabc: retinal vessel segmentation using adaboost, *IEEE Transactions on Information Technology in Biomedicine* 14 (5) (2010) 1267–1274.
- [57] X. You, Q. Peng, Y. Yuan, Y.-m. Cheung, J. Lei, Segmentation of retinal blood vessels using the radial projection and semi-supervised approach, *Pattern Recognition* 44 (10-11) (2011) 2314–2324.
- [58] D. Marín, A. Aquino, M. E. Gegúndez-Arias, J. M. Bravo, A new supervised method for blood vessel segmentation in retinal images by using gray-level and moment invariants-based features, *IEEE Transactions on Medical Imaging* 30 (1) (2011) 146–158.
- [59] Y. Wang, G. Ji, P. Lin, E. Trucco, Retinal vessel segmentation using multiwavelet kernels and multiscale hierarchical decomposition, *Pattern Recognition* 46 (8) (2013) 2117–2133.
- [60] A. M. Mendonca, A. Campilho, Segmentation of retinal blood vessels by combining the detection of centerlines and morphological reconstruction, *IEEE Transactions on Medical Imaging* 25 (9) (2006) 1200–1213.
- [61] M. A. Palomera-Pérez, M. E. Martínez-Pérez, H. Benítez-Pérez, J. L. Ortega-Arjona, Parallel multiscale feature extraction and region growing: application in retinal blood vessel detection, *IEEE Transactions on Information Technology in Biomedicine* 14 (2) (2010) 500–506.
- [62] M. E. Martínez-Pérez, A. D. Hughes, S. A. Thom, A. A. Bharath, K. H. Parker, Segmentation of blood vessels from red-free and fluorescein retinal images, *Medical Image Analysis* 11 (1) (2007) 47–61.
- [63] B. Al-Diri, A. Hunter, D. Steel, An active contour model for segmenting and measuring retinal vessels, *IEEE Transactions on Medical Imaging* 28 (9) (2009) 1488–1497.
- [64] M. Fraz, S. Barman, P. Remagnino, A. Hoppe, A. Basit, B. Uyyanonvara, A. Rudnicka, C. Owen, An approach to localize the retinal blood vessels using bit planes and centerline detection, *Computer Methods and Programs in Biomedicine* 108 (2) (2012) 600–616.
- [65] J. I. Orlando, M. Blaschko, Learning fully-connected CRFs for blood vessel segmentation in retinal images, in: *International Conference on Medical Image Computing and Computer-Assisted Intervention*, Boston, MA, USA, 2014, pp. 634–641.
- [66] J. Zhang, B. Dashtbozorg, E. Bekkers, J. P. Pluim, R. Duits, B. M. ter Haar Romeny, Robust retinal vessel segmentation via locally adaptive derivative frames in orientation scores, *IEEE Transactions on Medical Imaging* 35 (12) (2016) 2631–2644.
- [67] K. M. Brown, G. Barrionuevo, A. J. Canty, V. De Paola, J. A. Hirsch, G. S. Jefferis, J. Lu, M. Snippe, I. Sugihara, G. A. Ascoli, The DIADEM data sets: representative light microscopy images of neuronal morphology to advance automation of digital reconstructions, *Neuroinformatics* 9 (2-3) (2011) 143–157.